Chapter

Fluid Structure Interaction Analysis of Wind Turbine Rotor Blades Considering Different Temperatures and Rotation Velocities

Mayra K. Zezatti Flores, Laura Castro Gómez and Gustavo Urquiza

Abstract

Wind energy is the clean energy source that has had the highest installation growth worldwide. This energy uses the kinetic energy in the airflow currents to transform it into electrical energy through wind turbines. In this chapter, a rotor of a 2 MW of power wind turbine installed in Mexico is analyzed considering the wind velocity data and temperatures at each season of the year on the zone for the analysis in Computational Fluid Dynamics (CFD); subsequently, a Fluid–Structure Interaction (FSI) analysis was carried out to know the stress of the blades. The results show a relationship between temperature, air density, and power.

Keywords: FSI, wind turbine, CFD

1. Introduction

1.1 Wind energy in Mexico

Mexico has great potential for generating electricity from renewable resources. At the end of 2018, 75.88% of the energy used in the Mexican Republic comes from fossil fuels: such as oil, coal, and natural gas. Renewable energy generation reached 17.29% (hydroelectric, biogas, photovoltaic, wind, geothermal, and bagasse) and 6.83% from other clean energies (nuclear, efficient cogeneration, and black liquor) as illustrated in **Figure 1**, where it is observed the percentage distribution of total generation. There are currently 45 wind farms located in the country's eastern region (Oaxaca), where 59% of the total installed capacity is concentrated [1]. Also, other regions such as the northeast, northwest, western, peninsular, and Baja California.

Wind energy is generated from the kinetic energy in air currents and is transformed into electrical energy through wind turbines. Some important aspects for its generation are wind velocity and direction (Coriolis force), height, and temperature [2]. A minimum wind velocity of 3–5 m/s is required to start the rotor's rotation until reaching its maximum power.

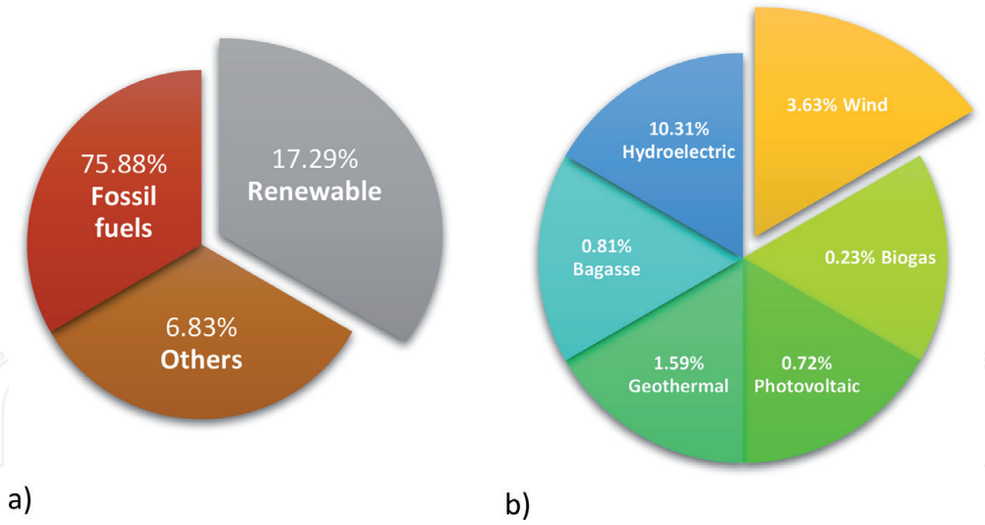

Figure 1.
(a) Distribution of total generation electricity in 2018 (b) renewable energy generation.

In the present work, a rotor of a wind turbine with a capacity of 2 MW is studied considering the real conditions of wind velocity at the temperatures presented in the year, first a Computational Fluid Dynamics (CFD) analysis, and subsequent a Fluid–Structure Interaction (FSI) analysis to know the stress of the blades of a turbine installed in a wind farm in the north of the country.

1.2 State of art

The rotor of a wind turbine is one of the most important components, for which it has been the object of study by some authors: Abolfazl Pourrajabian, carried out a study of the effect that air density has with respect to the torque of a small wind turbine of two meters in diameter, finding that the air density decreases as altitude increases, as well as the rotor torque [3]. Dong-Hoon Kim, studied a 5 MW turbine by means of fluid–structure, modeling in 2D only 1/3 of the rotor with different radial and longitudinal amplitudes of the rotary domain, considering a lineal composite material, obtaining the stress for a redesign of this [4]. Liping Dai, carried out a numerical study of the fluid structure of a Tjæreborg wind turbine, with a rotor diameter of 61.1 m, modeling a cylinder with the three blades to determine the behavior of deflection in a structural analysis, due to the effect of the velocity of wind with different angles of the YAW bearing [5]. Lanzafame analyzed a micro rotor of a horizontal axis turbine, to validate a BEM model in one dimension, comparing it with a CFD analysis performed in three dimensions; as a cylinder and two blades, and an experimental model, finding that the errors between simulated results in its power curve and the experimental data were less than 6% for all simulations [6]. With the previously analyzed studies, the characteristics, and conditions to carry out our case study were determined, such as domain dimensions, meshing with surface elements, turbulence model, wind velocity range, as well as the importance of determining the pressures. to perform a fluid–structure analysis.

2. Methodology

A wind turbine's operation is characterized by its power curve that indicates the range of wind velocities in which it can be operated and the one it generates.

(Eq. (1)) shows that the wind power depends on the swept area or the rotor exposed to a flow, as illustrated in **Figure 2**, on the fluid density and the wind

DOI: http://dx.doi.org/10.5772/intechopen.96495

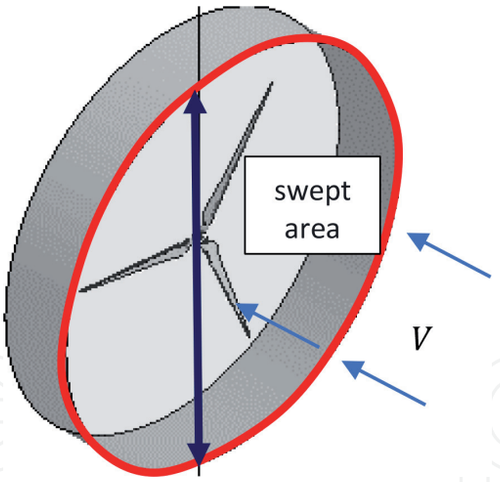

Figure 2.
Swept area of the blades of a wind turbine.

velocity. As Albert Betz demonstrated, wind energy is not used 100%; the limit he established was 59% for an ideal rotor. Additionally, the machine has mechanical, electrical, and aerodynamic losses [2, 7–9].

$$P = \frac{1}{2}\rho A V^3 \tag{1}$$

The Fluid–Structure Interaction (FSI) is the coupling of fluid and structural analysis. It considers the pressure or temperature of a CFD analysis and the direct consequences of this load on the structural analysis.

Two different software interact in the development of the fluid–structure analysis, where the independent fluid analysis is performed, and the required results are exported to the structural mesh for the solution. In this type of study, the CFD evaluation is solved in Fluent; then, the results are exported and imported to structural analysis, as illustrated in **Figure 3**.

2.1 CFD analysis

This analysis is carried out in three stages: pre-processing, processing, and post-processing. For the pre-processing development, the rotor geometry was generated

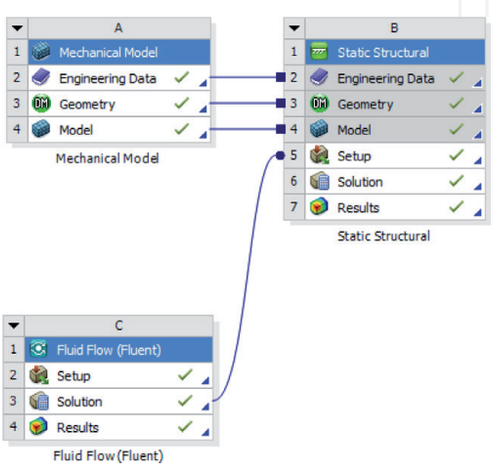

Figure 3.
Ansys diagram for the development of the FSI analysis.

in a CAD program from the information shown in **Table 1**, exported to another CAE program for the discretization.

Two domains were generated: rotary and stationary. **Figure 4** shows its dimensions, which were established according to the rotor diameter.

The discretization was carried out using an unstructured tetrahedral mesh. A refined mesh was realized in the zones near the rotatory interface and over the blade [10].

Were realized four meshes with different element sizes to perform an analysis of the independence of grid. This analysis consists of simulating at the same boundary conditions with a velocity inlet at 13 m/s and evaluating the torque results in these meshes.

It was calculated the percentage of relative error based on the torque result according to (Eq. (2)), considering the exact value of the one reported by the manufacturer in its power curve for a speed of 13 m/s, showing the values calculated in **Table 2**. According to the results, the mesh used has a relative error of 3.76%, illustrated in **Figure 5**, which shows the mesh in both domains.

$$Relative\ error = \frac{\left|V_{exact} - V_{approximate}\right|}{V_{exact}} \tag{2}$$

The definition of the physical models and solver configuration of the ANSYS Fluent software are shown in **Table 3**.

Statistical studies of the frequency for wind velocity and temperature were carried out (illustrated in **Figure 6**). The values of wind velocity are shown in the

Wind turbine	Characteristic
Diameter	87 m
Swept area	5,945 m^2
Rotation velocity	9–19 rpm
Profile	FFA + W3
Blade length	42.5 m
Design life	20 years

Table 1.
Rotor characteristics.

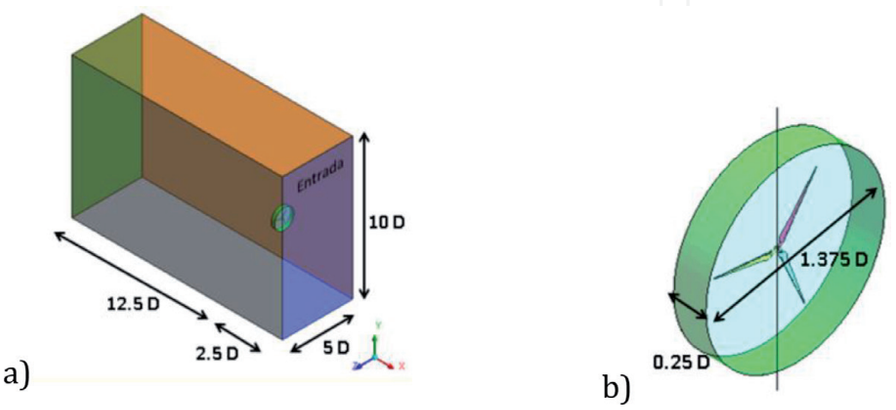

Figure 4.
Domain dimensions (a) stationary (b) rotary.

Type of mesh	Torque (N/m)	Relative error (%)
Reference (V_{exacto})	1,981,000	
Mesh1	1,647,193	16.85%
Mesh 2	1,696,181	14.38%
Mesh 3	1,906,495	3.76%
Mesh 4	1,865,284	5.84%

Table 2.
Calculation of the relative error.

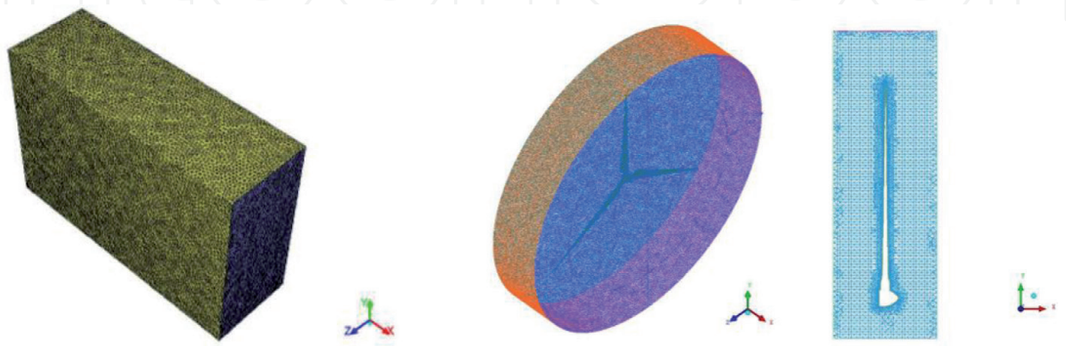

a) b)

Figure 5.
Meshed domain (a) stationary (b) rotary.

Configuration	Characteristic
Type of analysis	Stationary
Turbulence model	kω-sst
Interfaces	input, output, outline
Solution method	SIMPLE
Boundary conditions	Vel inlet, pressure output, wall, symmetry

Table 3.
Solver configuration.

red box of the histogram of the frequency. On the other hand, for the temperature, the data were obtained by taking an average for the months of each season of the year: spring 20°, summer 38°, autumn 15° and winter −5 ° C, verifying them with the maps of the National Meteorological Service of the same year during the months of each season and considering these temperature values for the properties of air in the CFD analysis.

Ten analyzes were carried out for each temperature value in a wind velocity range of 4–13 m/s. As shown in **Table 4**, using the characteristics described above, obtaining the torque calculates the mechanical power with the (Eq. (3)) and its respective angular velocity.

$$P = M\,\omega \tag{3}$$

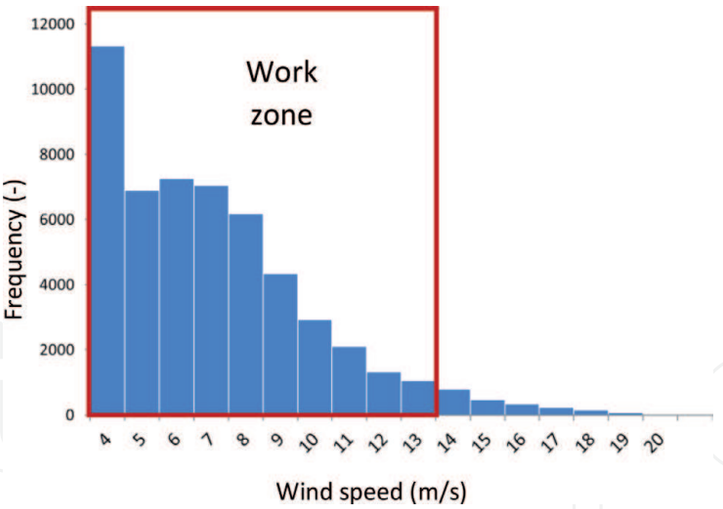

Figure 6.
Histogram of frequency of wind velocity during one year of operation.

Wind velocity (m/s)	Temperature (°C)
4	−5, 15, 20, 38
5	−5, 15, 20, 38
6	−5, 15, 20, 38
7	−5, 15, 20, 38
8	−5, 15, 20, 38
9	−5, 15, 20, 38
10	−5, 15, 20, 38
11	−5, 15, 20, 38
12	−5, 15, 20, 38
13	−5, 15, 20, 38

Table 4.
Operating conditions.

The post-processing of the results is presented in section 3.

2.2 FEM analysis

The rotor geometry is illustrated in **Figure 7a**, which was generated with surfaces following the data in **Table 1**, and **Figure 7b** demonstrates the thickness [11] imposed on the blades from root to the tip from 50 to 8 mm across the surface.

An analysis was performed with three different element sizes as seen in **Table 5**, with a rotational velocity of 19 rpm as a boundary condition to verify the maximum stress.

According to the results, it was decided to take mesh no.1 since the change in the data obtained is less than 5% with respect to mesh no.3. The numerical model of the rotor used is shown in **Figure 8**, which was carried out with second order elements shell281 [12].

The material of the hub and the blade was considered as a linear composite material [4]. As a boundary condition, support was imposed on the rotor hub and the rotational velocity in the direction of clockwise (Clockwise).

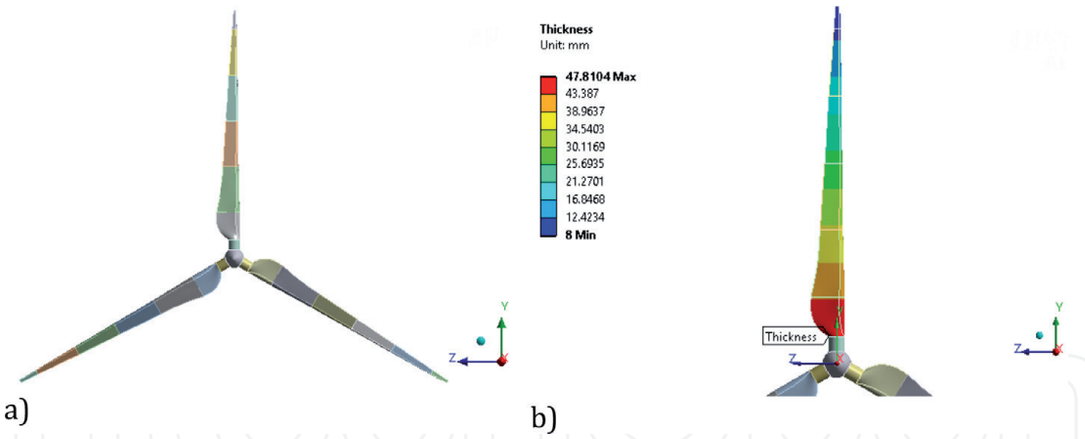

Figure 7.
Rotor characteristics (a) geometry (b) thickness distribution.

Mesh type	Number of nodes	Size element (mm)	Stress (MPa)
1	147,934	80	35.81
2	95,434	100	47.658
3	357,852	50	37.071

Table 5.
Von Mises stress results with different mesh sizes.

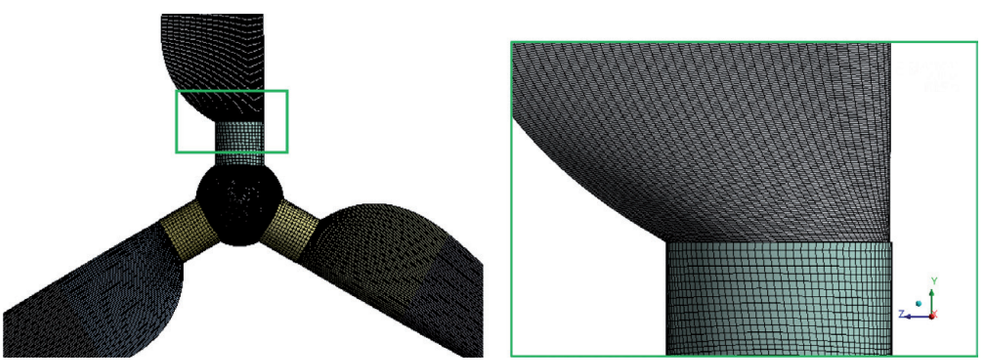

Figure 8.
Numerical rotor model.

Additionally, the evaluation's pressure results in CFD are included, imported to the structural analysis of each of the data obtained through interpolation of the ICEM mesh to the mesh generated in Ansys Workbench for the structural part.

The stress and strain results are shown in the next section.

3. Results

The CFD and FEM analysis simulation results are presented below, showing the mechanical power, pressures, and stress results, respectively.

3.1 CFD

Figure 9 shows four power curves, one curve for each temperature, and for each temperature ten analysis was performed for each value of wind speed in the range

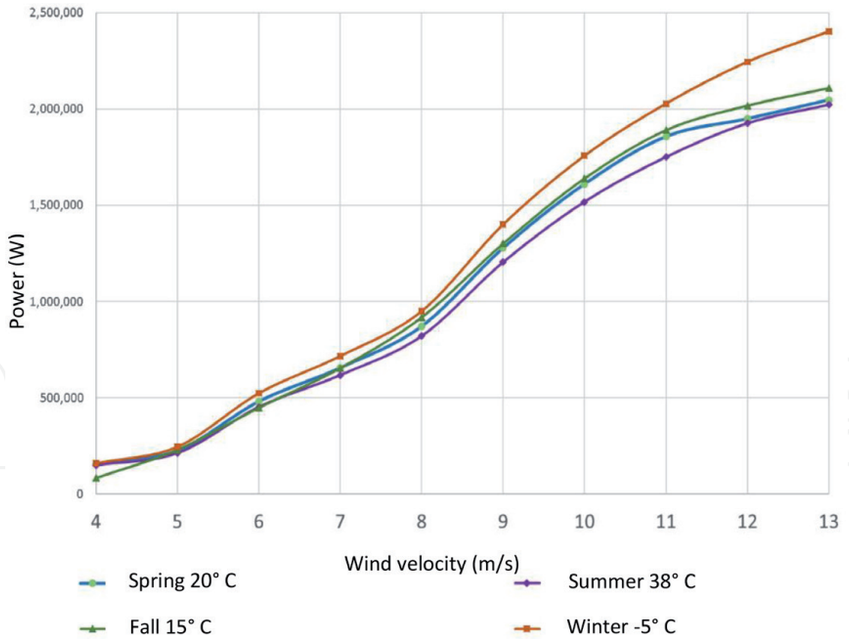

Figure 9.
Power at different temperatures.

of 4-13 m/s, obtaining a total of 40 simulations. The temperature directly affects the calculated power as seen in the figure, hence the air density [3].

When the temperature is increased, the air density decreases, and the power (Eq. (1)) shows that they are directly proportional.

The maximum power in the wind turbine area will be found during the winter when their temperature is −5 °C and the lowest during the summer that reaches 38 °C in the installed area.

The absolute pressure contour was obtained at all nodes on the rotor surface (**Figure 10**). The maximum stress is found at the edge of the profile outlet because the wind velocity is normal to the blade's plane, and as the profile rotates, it is the edge with the most significant impact.

3.2 FEM

An analysis was carried out at the different rotation velocitys in the operating range of 9–19 r.p.m. reported by the manufacturer. It can be noticed that the

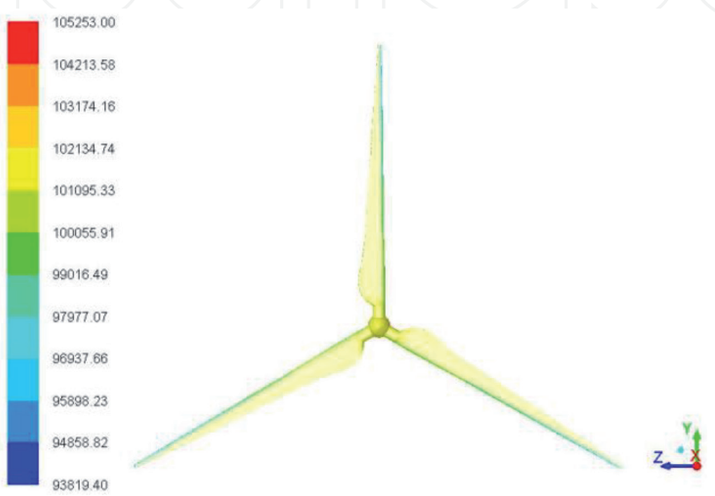

Figure 10.
Absolute pressure contour al blades (Pa).

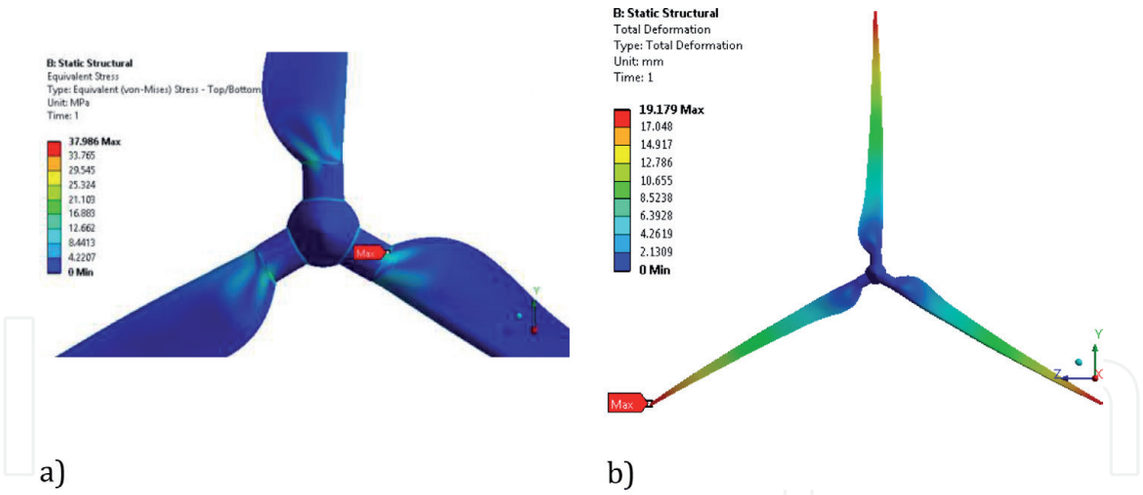

Figure 11.
Results at 19 r.p.m. (a) Von Mises stress state (b) maximum displacement.

contribution is minimal since the maximum stress of 8.5 MPa was obtained with the lower limit and 37.9 MPa with the upper limit.

The results at 19 r.p.m. are shown in **Figure 11**, in (a) the maximum stress distribution at the root of the blade in conjunction with the cylinder due to the change in thickness and b) the maximum displacement found at the tip of the blade.

3.3 FSI

The obtained pressures were exported to ANSYS Mechanical at each wind velocity for its structural analysis, adding the mentioned boundary conditions to obtain a stress state.

The state of stress at different temperatures in the predominant velocity range of 4-13 m/s show in **Figure 12**. It is observed that at 38 °C during the summer, the stresses are less than during the winter, at −5 °C. The centrifugal force contributes approximately 30% of the total effort with the pressure exerted by the air on the rotor's surface.

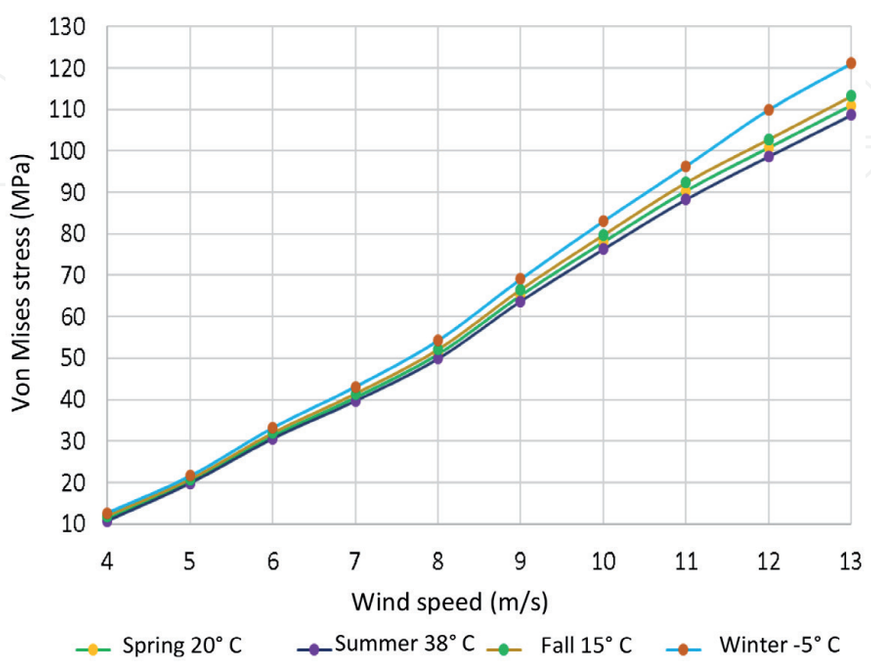

Figure 12.
Von Mises stresses at different temperatures.

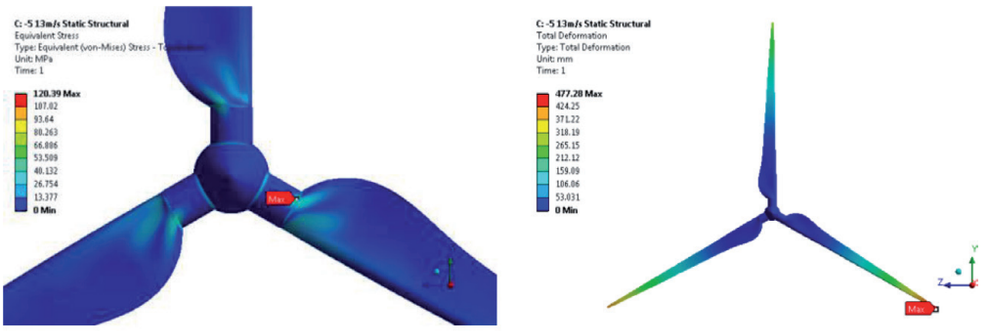

a) b)

Figure 13.
Rotor results at 13 m/s. (a) Von Mises stress state (b) maximum displacement.

Figure 13(a) shows the Von Mises stress distribution at a maximum wind velocity of 13 m/s, in which the blade root zone is affected by the bending of the blade tip, and on (b) illustrates the maximum displacement located at the tip of the blade, where the effect of the rotation and the pressure of the air entering to the surface affects the area with the minimum thickness.

4. Conclusions

The CFD methodology used in the present work was validated by comparing the results between the calculated power with the manufacturer power, obtaining a valid approximation to the real phenomenon, taking into account the ideality of the case under study, in addition to not considering the aerodynamic, mechanical and electrical losses of the wind-power generator.

Was performed ten CFD simulations for each value of temperature to obtain the pressures for the structural analyses. It was demonstrated that the mechanical power has a directly proportional relationship with the temperature and with the air density, with which it is concluded that the maximum power in the year is generated during the winter, average power in summer and autumn, and a minimum power in the summer in the installation area.

The fluid–structure analyses include the forty simulations performed for CFD's and the stress for the structural analysis at different rotation velocities. The maximum stress was found at 13 m/s, lower for 38 °C and higher for −5 °C, located mainly at the blade's root due to the change in thickness and rotation velocity and the pressure exerted by the air. Which 120 MPa does not exceed the yield stress of 240 MPa.

DOI: http://dx.doi.org/10.5772/intechopen.96495

IntechOpen

Author details

Mayra K. Zezatti Flores, Laura Castro Gómez* and Gustavo Urquiza
Autonomous University of Morelos State (UAEM), Morelos, Mexico

*Address all correspondence to: lauracg@uaem.mx

References

[1] SENER, "Reporte de Avance de Energías Limpias Primer Semestre 2018," México, 2018.

[2] W. Tong et. al., "Wind Power Generation and Wind Turbine Design," *WIT press,* pp. ISBN 978-1-84564-205-1, 2010.

[3] Abolfazl Pourrajabian et. al., "Effect of air density on the performance of a small wind turbine blade: A case study in Iran," *Wind Eng. Ind. Aerodyn.,* pp. 1-10 p. DOI: doi.org/10.1016/j.jweia.2014.01.001, 126, 2014.

[4] Dong-Hoon Kim et. al., "Optimization of 5-MW wind turbine blade using fluid structure interaction analysis," *Mechanical Science and Technology,* pp. 725-732 p. DOI: doi.org/10.1007/s12206-017-0124-2, 2017.

[5] Liping Dai, et. al., "Analysis of wind turbine blades aeroelastic performance under yaw conditions," *Journal of Wind Engineering & Industrial Aerodynamics,* vol. 171, pp. 237-287 DOI: doi.org/10.1016/j.jweia.2017.09.011, 2017.

[6] Lanzafame et. al., "Wind turbine CFD modeling using a correlation-based transitional model," *Renewable Energy,* vol. 52, pp. 31-39 DOI:doi.org/10.1016/j.renene.2012.10.007, 2013.

[7] M. F. Voneschen, Introducción a la teoría de las turbinas eólicas, España: LA VERITAT ISBN 3-7625-2700-8 , 2009.

[8] A. Betz, La energía eólica y su aprovechamiento mediante molinos de viento, traducido por Manuel Franquesa Voneschen, 2012.

[9] A. P. Schaffarczyk, "Introduction to wind turbine aerodynamics", Alemania: Springer DOI 10.1007/978-3-642-36409-9, 2014.

[10] J.M. O'Brien et. al., "Horizontal axis wind turbine research: A review of commercial CFD, FE codes and experimental practices," *Progress in Aerospace Sciences,* pp. 1-24 p. DOI: doi.org/10.1016/j.paerosci.2017.05.001, 2017.

[11] Jin Chen, et. al., "Structural optimization study of composite wind turbine blade," *Materials and Design,* pp. 247-255 p. DOI: doi.org/10.1016/j.matdes.2012.10.036, 2013.

[12] *Ansys user's guide,* 2019.